Design of a Piezoelectric Actuated Microgripper with a Three-Stage Flexure-Based Amplification

Fujun Wang, Cunman Liang, Yanling Tian, Member, IEEE, Xingyu Zhao, and Dawei Zhang

***Abstract*—This paper presents a novel microgripper mechanism for micro manipulation and assembly. The microgripper is driven by a piezoelectric actuator, and a three-stage flexure-based amplification has been designed to achieve large jaw displacements. The kinematic, static and dynamic models of the microgripper have been established and optimized considering the crucial parameters that determine the characteristics of the microgripper. Finite element analysis (FEA) was conducted to evaluate the characteristics of the microgripper, and wire Electro Discharge Machining (EDM) technique was utilized to fabricate the monolithic structure of the microgripper mechanism. Experimental tests were carried out to investigate the performance of the microgripper and the results show that the microgripper can grasp micro objects with a maximum jaw motion stroke of 190 μm corresponding to the 100 V applied voltage. It has an amplification ratio of 22.8 and working mode frequency of 953 Hz.**

***Index Terms*—Microgripper, Flexure-based amplification, Modeling, Optimization design**

I. Introduction

RECENTLY the trend towards miniaturizing products such as Micro-Electro-Mechanical System(MEMS) has stimulated extensive research on automated micro manipulation and assembly techniques [1]-[6], and the development of miniaturized system for manipulating and assembling micro objects has become a great challenge for the precision engineering future [7]. Compared with other contact and contactless micro manipulation and assembly techniques, such as optical, electrostatic, Bernoulli, ultrasonic and magnetic, microgrippers are more preferred, because of their ability to grasp different shaped objects with high precision and low cost [8]. They have many applications in microelectronics, material science, biology and tissue engineering and etc [9]. As a result, it is necessary to develop novel microgrippers with high performance to satisfy the stringent performance requirements of modern micro manipulation and assemble operations.

Several studies have been reported on the design of microgrippers with different specifications. Among the research, two major components during design process, namely actuation principles and displacement transmission mechanisms, have been commonly emphasized [10].

The development of novel actuation principles improves the gripper performance, and there are four major actuation techniques typically used in micro grasping operations. Beyeler et al. [11] and Chen et al. [12] designed electrostatic comb actuated MEMS microgrippers with a motion stroke of more than 100 μm. However, the electrostatic grippers can usually generate small grasping forces. Kim et al. [13] and Chronis et al. [14] presented electrothermal microgrippers, but the electrothermal actuators have the drawbacks of high operation temperature, nonlinear movement and low sensitivity. Shaped memory alloy actuators have been utilized by Kohl at al.[15] and Roch at al. [16] for microgrippers, but short lifetime, hysteresis and high response time limit their further applications. Due to the inherent advantages such as high force output to weight ratio, fast response and zero backlash, piezoelectric(PZT) actuators have been widely used in precision positioning system and microgrippers [17]-[19], and good performance can be achieved with proper control of such kinds of piezoelectric actuated systems [20]-[22].

As a critical component of microgrippers, displacement transmission mechanism (DTM) has an important effect on the microgripper characteristics. Because the output displacement of the actuator is small, it is usually amplified by DTMs [23]. Several PZT actuated microgrippers with different DTMs have been developed. Sun et al. [24] and Zubir et al. [25] designed piezoelectric driven compliant-based microgrippers for micromanipulation, both of which had low amplification ratios and thus the jaw displacements were confined. A monolithic compliant PZT driven microgripper was designed by Wang et al. [26], and a larger displacement amplification ratio was achieved. However, the microgripper dynamic characteristics were not presented. To improve the efficiency and quality of micro manipulation and assembly, this paper presents the design, modeling, optimization, fabrication and experimental test of a novel piezoelectric actuated microgripper with a three-stage flexure-based amplification.

Manuscript received on July 03, 2014. This work was supported in part by the National Natural Science Foundation of China under Grant 51205279, 51275337 and 51175372, in part by the Science & Technology Commission of Tianjin Municipality under Grant no. 13JCQNJC04100, the Tianjin University for Peiyang Elite Scholar under Grant no. 60301014 and CSC Scholarship.

F. J. Wang is with Tianjin Key Laboratory of Equipment Design and Manufacturing Technology, School of Mechanical Engineering, Tianjin University, Tianjin 300072, China and Center for Nanoscale Chemical-Electrical-Mechanical Manufacturing Systems, Department of Mechanical Science and Engineering, University of Illinois at Urbana-Champaign, Urbana 61801, USA. (email: wangfujun@tju.edu.cn)

C. M. Liang, Y. L. Tian, X. Y. Zhao, and D. W. Zhang are with Tianjin Key Laboratory of Equipment Design and Manufacturing Technology, School of Mechanical Engineering, Tianjin University, Tianjin 300072, China (email: lcm@tju.edu.cn, meytian@tju.edu.cn, zxytju@tju.edu.cn, medzhang@tju.edu.cn)

The rest of the paper is organized as follows: Section II introduces the micrograpper mechanism. In section III, the modeling and optimization design are carried out. Then the micrograpper characteristics are analyzed in section IV. After that the experiments are presented in Section V to investigate the performance of the developed micrograpper. Finally, Section VI concludes this paper.

II. Mechanism of the Micrograpper

Figure 1 shows the mechanism of the piezoelectric actuated flexure-based micrograpper consisting of a stack piezoelectric ceramic actuator (SPCA), a pair of grasping jaws, a preload bolt, a base and a displacement transmission mechanism. In order to get large jaw displacements, the DTM is designed as a three-stage flexure-based amplification including a homothetic bridge type mechanism and two leverage mechanisms. Right circular flexure hinges are more precise in keeping the positions of the rotation centers compared to the others, so they are selected for the flexure-based amplification [26]. The SPCA is connected with the DTM by the preload bolt at one end of the SPCA, and the preload force to the SPCA can be adjusted through the bolt. Both of the grasping jaws are fixed on the base, and the micrograpper is designed symmetrically along the longitudinal axis of piezoelectric actuator to avoid shear force and bending torque acting on the piezoelectric actuator.

The motion transmission is realized through the three-stage amplification. The homothetic bridge-type mechanism is composed of the connecting rod mechanisms (A-B-C-D; A'-B'-C'-D') based on the double-notch right circular flexure hinges. In order to obtain a large amplification ratio, there are two leverage mechanisms (E-F-G and E'-F'-G'; H-I and H'-I') at each side of the micrograppe also based on the double-notch right circular flexure hinges. Using the three-stage amplification, large jaw displacements can be achieved under a small displacement of the piezoelectric actuator. In order to grasp an object, a voltage should be applied to the SPCA to make it expand which will push the homothetic bridge-type mechanism (A-B-C-D; A'-B'-C'-D'); then the homothetic bridge-type mechanism will pull the leverage mechanisms (E-F-G and E'-F'-G'; H-I and H'-I'), causing the grasping jaws to close to grasp the manipulated objects. After power is switched off, the SPCA retracts to its initial position, causing the grasping jaws to open and release the manipulated objects.

III. Modeling and Optimization Design

A. Kinematic modeling

Assuming that: 1) the elastic deformations of the micrograpper only occur at the flexure hinges and the other components are considered as rigid bodies, and 2) the flexure hinge deformations are assumed to be pure bending and the rotational angle is small (generally less than 1°) without any

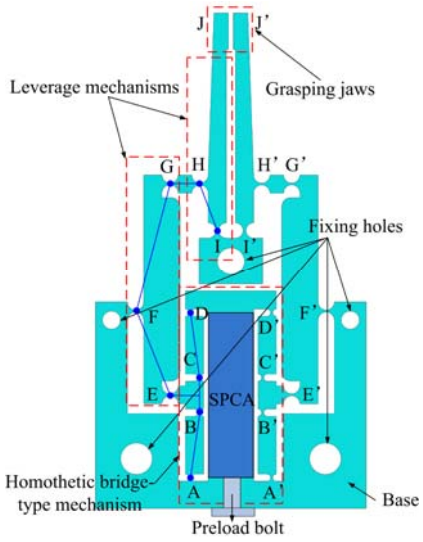

Fig. 1. Schematic diagram of the piezoelectric driven micrograpper.

expansion and contraction deformations [24], [27]. According to the Pseudo Rigid Body Model (PRBM) approach, the equivalent model of the piezoelectric actuated micrograpper can be achieved and shown in Fig. 2, where i (i =A, B... I) denotes the rotational centers of flexure hinges, and d_{in} and d_{out} are the input displacement from the SPCA and the output displacement of the grasping jaw, respectively.

A-B-C-D-E-F is equivalent to a six-bar linkage mechanism and F-G-H-I is considered as a four-bar linkage mechanism as shown in Fig. 2(b). In the six-bar linkage mechanism, the linkages AB, BC, CD and FE have the initial angular positions of φ_1, φ_2, φ_3, and φ_4, respectively. L_i (i=AB, BC,..., AF) are the lengths of the linkages, S is the initial displacement of point D, α is the angle between linkages BC and BE, and the linkage AF has the angle β from the x-axis positive direction. Based on the geometric and motion relationships, the following equations can be gotten:

$$l_{AB}e^{i\varphi_1} + l_{BE}e^{i(\varphi_2+\alpha)} = l_{AF}e^{i\beta} + l_{FE}e^{i\varphi_4} \tag{1}$$

$$l_{AB}e^{i\varphi_1} + l_{BC}e^{i\varphi_2} + l_{CD}e^{i\varphi_3} = Se^{i\frac{\pi}{2}} \tag{2}$$

Differentiating Eqs (1) and (2) with respect to time, yields

$$l_{AB}\omega_1 e^{i(\varphi_1+\frac{\pi}{2})} + l_{BE}\omega_2 e^{i(\varphi_2+\alpha+\frac{\pi}{2})} = l_{FE}\omega_4 e^{i(\varphi_4+\frac{\pi}{2})} \tag{3}$$

$$l_{AB}\omega_1 e^{i(\varphi_1+\frac{\pi}{2})} + l_{BC}\omega_2 e^{i(\varphi_2+\frac{\pi}{2})} + l_{CD}\omega_3 e^{i(\varphi_3+\frac{\pi}{2})} = \dot{S}e^{i\frac{\pi}{2}} \tag{4}$$

where $\alpha = \arctan\left(2l_3 / l_{BC}\right)$.

Let the real and imaginary parts be equal, respectively, and thus the following equations can be obtained:

$$l_{AB}\omega_1 \sin\varphi_1 + l_{BE}\omega_2 \sin(\varphi_2+\alpha) = l_{FE}\omega_4 \sin\varphi_4 \tag{5}$$

$$l_{AB}\omega_1 \cos\varphi_1 + l_{BE}\omega_2 \cos(\varphi_2+\alpha) = l_{FE}\omega_4 \cos\varphi_4 \tag{6}$$

$$l_{AB}\omega_1 \sin\varphi_1 + l_{BC}\omega_2 \sin\varphi_2 + l_{CD}\omega_3 \sin\varphi_3 = 0 \quad (7)$$

$$l_{AB}\omega_1 \cos\varphi_1 + l_{BC}\omega_2 \cos\varphi_2 + l_{CD}\omega_3 \cos\varphi_3 = \dot{S} \quad (8)$$

From Eqs (5)-(8), the following relationship can be written:

$$\omega_4 = b\omega_1 \quad (9)$$

$$l_{AB}\omega_1 \cos\varphi_1 + l_{BC}\omega_2 \cos\varphi_2 + l_{CD}\omega_3 \cos\varphi_3 = \dot{S} \quad (10)$$

where $a = -\dfrac{l_{AB}\sin(\varphi_1 - \varphi_4)}{l_{BE}\sin(\varphi_2 + \alpha - \varphi_4)}$, $b = \dfrac{l_{AB}\sin(\varphi_1 - \varphi_2 - \alpha)}{l_{EF}\sin(\varphi_4 - \varphi_2 - \alpha)}$, and $c = -\dfrac{l_{AB}\sin\varphi_1 + a l_{BC}\sin\varphi_2}{l_{CD}\sin\varphi_3}$.

In the four-bar linkage mechanism, the linkages FG, GH and HI have the initial angular positions of φ_5, φ_6, and φ_7, respectively. The length of the linkages is L_i (i=FG, GH, IH, FI, IJ). The linkage IH has the angle γ from the x-axis positive direction. Based on the geometric and motion relationships, the following equation can be obtained:

$$l_{FG}e^{i\varphi_5} + l_{GH}e^{i\varphi_6} = l_{FI}e^{i\gamma} + l_{IH}e^{i\varphi_7} \quad (11)$$

Differentiating Eq. (11) with respect to time, yields

$$l_{FG}\omega_5 e^{i(\varphi_5+\frac{\pi}{2})} + l_{GH}\omega_6 e^{i(\varphi_6+\frac{\pi}{2})} = l_{IH}\omega_7 e^{i(\varphi_7+\frac{\pi}{2})} \quad (12)$$

Let the real and imaginary parts of Eq.(12) be equal, respectively and the following equations can be achieved:

$$l_{FG}\omega_5 \sin\varphi_5 + l_{GH}\omega_6 \sin\varphi_6 = l_{IH}\omega_7 \sin\varphi_7 \quad (13)$$

$$l_{FG}\omega_5 \cos\varphi_5 + l_{GH}\omega_6 \cos\varphi_6 = l_{IH}\omega_7 \cos\varphi_7 \quad (14)$$

The following relationship can be gotten:

$$\omega_7 = \frac{l_{FG}\sin(\varphi_5 - \varphi_6)}{l_{HI}\sin(\varphi_7 - \varphi_6)}\omega_5 \quad (15)$$

$$\omega_5 = \omega_4 = b\omega_1 \quad (16)$$

Thus

$$\omega_7 = \frac{l_{FG}\sin(\varphi_5 - \varphi_6)}{l_{HI}\sin(\varphi_7 - \varphi_6)}\omega_5 \quad (17)$$

The displacement amplification ratio R_{amp} of the microgripper is defined as

$$R_{amp} = \frac{2\partial d_{out}}{\partial d_{in}} \quad (18)$$

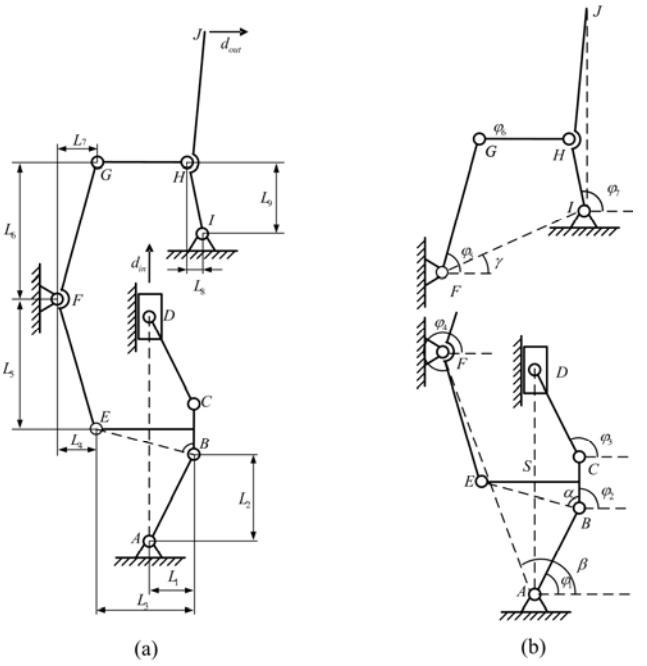

Fig. 2. Pseudorigid-body-model of the piezoelectric driven microgripper: (a) the schematic diagram and (b) the displacement diagram.

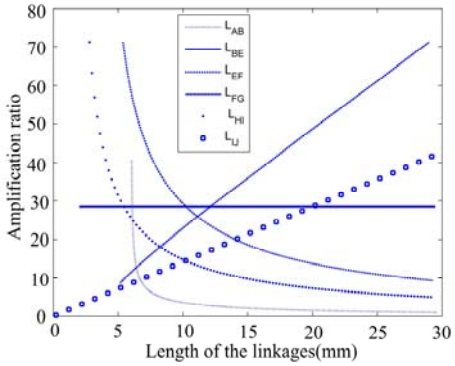

Fig. 3. The amplification ratio varies with the lengths of the linkages.

where ∂d_{out} and ∂d_{in} are the small displacements of the single jaw and input end, respectively.

The velocities of points D and J can be written as

$$v_D = \frac{\partial d_{in}}{\partial t} = \dot{S} \quad (19)$$

$$v_J = \frac{\partial d_{out}}{\partial t} = \omega_7 l_{IJ} \quad (20)$$

The displacement amplification ratio can be calculated as

$$R_{amp} = \frac{2\partial d_{out}}{\partial d_{in}} = 2\frac{\partial d_{out}/\partial t}{\partial d_{in}/\partial t} = \frac{2v_J}{v_D} \quad (21)$$

Substituting Eqs (10), (17) and (20) into Eq.(21), yields

$$R_{amp} = \frac{2bl_{IJ}l_{FG}\sin(\varphi_5 - \varphi_6)}{(l_{HI}\sin(\varphi_7 - \varphi_6))(l_{AB}\cos\varphi_1 + al_{BC}\cos\varphi_2 + cl_{CD}\cos\varphi_3)} \tag{22}$$

Eq. (22) shows that the amplification ratio is mainly determined by the length of each linkage. The influence of the linkage lengths on the amplification ratio is analyzed and summarized in Fig.3. The amplification ratio increases with l_{FG} and l_{IJ} increasing and decreases as l_{AB}, l_{EF} and l_{HI} increase. l_{BE} has no effect on the amplification ratio.

B. Static modeling

When a small displacement d_{in} from the SPCA is applied to the input terminal of the microgripper, the angle increment of each moving linkage can be obtained. Furthermore, the rotational angles of the flexure hinges can be calculated as

$$\psi_A = \frac{d_{in}}{\varepsilon} \tag{23}$$

$$\psi_B = \frac{ad_{in}}{\varepsilon} - \frac{d_{in}}{\varepsilon} = \frac{(a-1)d_{in}}{\varepsilon} \tag{24}$$

$$\psi_C = \frac{cd_{in}}{\varepsilon} - \frac{ad_{in}}{\varepsilon} - \frac{d_{in}}{\varepsilon} = \frac{(c-a-1)d_{in}}{\varepsilon} \tag{25}$$

$$\psi_D = \frac{d_{in}}{\varepsilon} + \frac{(a-1)d_{in}}{\varepsilon} + \frac{(c-a-1)d_{in}}{\varepsilon} = \frac{(c-1)d_{in}}{\varepsilon} \tag{26}$$

$$\psi_F = \frac{bd_{in}}{\varepsilon} \tag{27}$$

$$\psi_E = -\psi_A - \psi_B + \psi_F = \frac{(b-a)d_{in}}{\varepsilon} \tag{28}$$

$$\psi_G = -\frac{bl_{FG}\sin(\varphi_5 - \varphi_7)}{l_{GH}\sin(\varphi_6 - \varphi_7)\varepsilon}d_{in} - \frac{b}{\varepsilon}d_{in} \tag{29}$$

$$\psi_I = \frac{bl_{FG}\sin(\varphi_5 - \varphi_6)d_{in}}{l_{HI}\sin(\varphi_7 - \varphi_6)\varepsilon} \tag{30}$$

where $\varepsilon = l_{AB}\cos\varphi_1 + al_{BC}\cos\varphi_2 + cl_{CD}\cos\varphi_3$, and the negative signs of the angles indicate that the rotational motion of flexure hinge is in the clockwise direction.

Based on the PRBM approach, the static modeling is carried out to describe the force-deflection relationship of flexure hinges. The microgripper will be subsequently transformed into rigid body mechanism by replacing the flexible segment into equivalent rigid joint and torsional spring. This approach will simplify the model to enable conventional rigid body kinematic analysis to be performed for further investigation on the gripper performance and acquiring various critical design parameters.

The torsional spring constant of the flexural hinge can be estimated by

$$K_{ri} = \frac{2EBt_i^{5/2}}{9\pi r_i^{1/2}} \quad i = A,...,I \tag{31}$$

where r_i and t_i are the radius and thickness of the ith flexure hinge, respectively, E is the elastic modulus of the material, and B is the thickness of the microgripper.

Since the flexure hinges in the homothetic bridge-type mechanism should be the same to maintain symmetry, r_1 is defined as the radius of flexure hinges in the homothetic bridge-type mechanism, and r_2 is the radius of the other flexure hinges.

Furthermore, the torque M_i, generated at the rotational center of the flexure hinge, can be obtained as

$$M_i = -K_{ri}\psi_i \quad i = A,...,I \tag{32}$$

where the negative sign indicates that the torque has the opposite direction with the rotational motion of flexure hinges.

In order to derive the input stiffness of the microgripper, the Castigliano's first theorem is adopted and expressed as

$$F_{in} = \frac{\partial U}{\partial d_{in}} \tag{33}$$

where d_{in} is the deformation due to the applied force, F_{in} is the applied force, and U is the deformation energy and given as

$$U = \frac{1}{2}\sum_{i=A}^{I} K_{ri}\psi_i^2 \tag{34}$$

Substituting Eqs(23)-(30) into Eq.(34), yields

$$\begin{aligned} U = {} & \frac{K_{rA}}{2\varepsilon^2}d_{in}^2 + \frac{K_{rB}(a-1)^2}{2\varepsilon^2}d_{in}^2 + \frac{K_{rC}(c-a-1)^2}{2\varepsilon^2}d_{in}^2 \\ & + \frac{K_{rD}(c-1)^2}{2\varepsilon^2}d_{in}^2 + \frac{K_{rE}(b-a)^2}{2\varepsilon^2}d_{in}^2 + \frac{K_{rF}b^2}{2\varepsilon^2}d_{in}^2 \\ & + \frac{K_{rG}\xi_1^2}{2\varepsilon^2}d_{in}^2 + \frac{K_{rH}\xi_2^2}{2\varepsilon^2}d_{in}^2 + \frac{K_{rI}\xi_3^2}{2\varepsilon^2}d_{in}^2 \end{aligned} \tag{35}$$

where $\xi_1 = -\frac{bl_{FG}\sin(\varphi_5 - \varphi_7)}{l_{GH}\sin(\varphi_6 - \varphi_7)} - b$, $\xi_2 = \frac{bl_{FG}\sin(\varphi_5 - \varphi_6)}{l_{HI}\sin(\varphi_7 - \varphi_6)}$, and $\xi_3 = \frac{bl_{FG}\sin(\varphi_5 - \varphi_7)}{l_{GH}\sin(\varphi_6 - \varphi_7)} + \frac{bl_{FG}\sin(\varphi_5 - \varphi_6)}{l_{HI}\sin(\varphi_7 - \varphi_6)}$.

The applied force can be expressed as

$$F_{in} = \frac{\partial U}{\partial d_{in}} = \left(\begin{aligned} & \frac{K_{rA}}{\varepsilon^2} + \frac{K_{rB}(a-1)^2}{\varepsilon^2} + \frac{K_{rC}(c-a-1)^2}{\varepsilon^2} + \frac{K_{rD}(c-1)^2}{\varepsilon^2} \\ & + \frac{K_{rE}(b-a)^2}{\varepsilon^2} + \frac{K_{rF}b^2}{\varepsilon^2} + \frac{K_{rG}\xi_1^2}{\varepsilon^2} + \frac{K_{rH}\xi_2^2}{\varepsilon^2} + \frac{K_{rI}\xi_3^2}{\varepsilon^2} \end{aligned} \right) d_{in} \tag{36}$$

The input stiffness of the microgripper can be derived as

$$K_{in} = \frac{F_{in}}{d_{in}} = \frac{K_{rA}}{\varepsilon^2} + \frac{K_{rB}(a-1)^2}{\varepsilon^2} + \frac{K_{rC}(c-a-1)^2}{\varepsilon^2} + \frac{K_{rD}(c-1)^2}{\varepsilon^2} + \frac{K_{rE}(b-a)^2}{\varepsilon^2} + \frac{K_{rF}b^2}{\varepsilon^2} + \frac{K_{rG}\xi_1^2}{\varepsilon^2} + \frac{K_{rH}\xi_2^2}{\varepsilon^2} + \frac{K_{rI}\xi_3^2}{\varepsilon^2} \quad (37)$$

From Eq. (37), it can be seen that the input stiffness of the microgripper depends on its geometrical parameters.

Considering the PRBM of the microgripper with external forces on the input terminal and jaw, and torques at each joint, the following equation can be obtained based on the force equilibrium of the microgripper:

$$F_{in} = K_{in}d_{in} + \frac{R_{amp}}{2}F_{out} = \frac{2K_{in}d_{out}}{R_{amp}} + \frac{R_{amp}}{2}F_{out} \quad (38)$$

Eq. (38) describes the relationship among the output force, the input force, input displacement and displacement amplification ratio of the microgripper. The larger the amplification ratio R_{amp}, the smaller the output force F_{out}. When the microgripper does not grasp the manipulated object, the output displacement is determined by the geometrical parameters of the microgripper and the input force. While grasping the manipulated object, the output displacement does not change when increasing the input force and the input displacement because the gripping jaws are fixed. Generally, the grasping jaws will close and then grasp the manipulated object with increasing voltage applied to the microgripper.

To evaluate the stress concentration at each flexure hinge, the reaction force and torque of each flexure hinge are determined and shown in Fig.4. Through the static equilibrium analysis of each rigid linkage, the following equations can be obtained:

$$F_{Ay} = F_{By} = F_{Cy} - F_{Ey} \quad (39)$$

$$F_{Ax} = F_{Bx} = F_{Cx} - F_{Ex} \quad (40)$$

$$F_{Dy} = -F_{Cy} = F_{in} \quad (41)$$

$$F_{Dx} = -F_{Cy} = \frac{M_C + M_D - F_{Dy}L_1}{L_2} \quad (42)$$

$$F_{Ex} = \frac{2(M_2L_3 - M_1L_4)}{2L_5L_3 - L_{BC}L_4} \quad (43)$$

$$F_{Ey} = \frac{M_2L_3 - F_{Ex}L_5}{L_4} \quad (44)$$

$$F_{Fx} = F_{Ex} + F_{Gx} \quad (45)$$

$$F_{Fy} = F_{Ey} + F_{Gy} \quad (46)$$

$$F_{Gx} = -F_{Hx} = -F_{Ix} = \frac{M_I + F_{Hy}L_8 + F_{out}L - M_H}{L_9} \quad (47)$$

$$F_{Gy} = -F_{Hy} = -F_{Iy} = \frac{M_G + M_H}{L_{GH}} \quad (48)$$

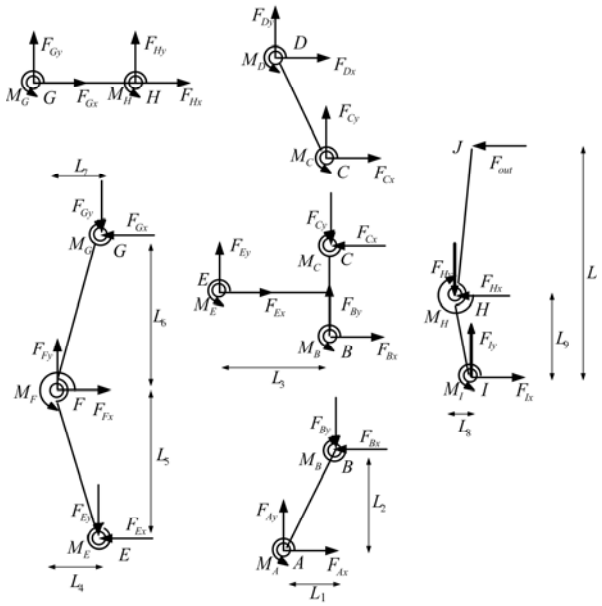

Fig. 4. Static body analysis of the piezoelectric actuated microgripper.

The maximum stress σ_{max} occurs at the outer surface of the thinnest part of each flexure hinge, and can be expressed as

$$(\sigma_{max})_i = \left|\frac{4Et_i^{1/2}\psi_i}{3\pi r_i^{1/2}}\right| + \left|\frac{F_{iy}}{bt_i}\right| \qquad i = A,B,C,D,I \quad (49)$$

$$(\sigma_{max})_i = \left|\frac{4Et_i^{1/2}\psi_i}{3\pi r_i^{1/2}}\right| + \left|\frac{F_{ix}}{bt_i}\right| \qquad i = E,F,G,H \quad (50)$$

Here, the maximum allowable stress is considered. Thus

$$(\sigma_{max})_i < \frac{[\sigma]}{n_a} \quad (51)$$

where $[\sigma]$ denotes the tensile yield stress, and n_a (n_a >1) represents the factor of safety.

C. Dynamic modeling

The natural frequencies can be derived using Lagrange's equation expressed as

$$\frac{d}{dt}\left(\frac{\partial T}{\partial \dot{q}_i}\right) - \frac{\partial T}{\partial q_i} + \frac{\partial V}{\partial q_i} = F_i \qquad i = 1,2,...,n, \quad (52)$$

where T and V denote the total kinetic energy and potential energy of the system, respectively, q_i is the generalized coordinate, n is the number of generalized coordinates and F_i represents the generalized nonconservative force.

The kinetic energy of the entire system can be expressed as

$$T = \frac{1}{2}(m_{in} + m_{SPCA})\dot{x}_{in}^2 + I_{AB}\omega_1^2 + I_{CD}\omega_1^2 + (I_{FE} + I_{FG})\omega_4^2 + I_{IJ}\omega_7^2 + m_{BCE}\dot{x}_E^2 + m_{GH}x_H^2 \quad (53)$$

where m_{SPCA} is the mass of the SPCA, m_{in} is the mass of the microgripper input terminal. m_{BCE} and m_{GH} are the masses of the rigid frames BCE and GH, respectively, I_{AB}, I_{CD}, I_{EF}, I_{FG}, and I_{IJ} represent the moments of inertia of the linkages AB, CD, EF, FG and IJ with respect to their corresponding instantaneous centers, respectively.

The potential energy of the entire system is expressed as

$$V = \sum_{i=A}^{I} k_i \psi_i^2 + \frac{1}{2}k_{SPCA}x_{in}^2 \quad (54)$$

where k_i is the rotational stiffness of the flexure hinge I and k_{SPCA} is the stiffness of the SPCA.

The dynamic model of the microgripper can be expressed as

$$M\ddot{x}_{in} + Kx_{in} = F \quad (55)$$

where

$$M = m_{in} + m_{SPCA} + \frac{2(I_{AB}+I_{CD})}{\varepsilon^2} + \frac{2b^2(I_{FE}+I_{FG})}{\varepsilon^2} + \frac{2\xi_3^2 I_{IJ}}{\varepsilon^2} + \frac{2m_{BCE}L_{EF}^2}{\varepsilon^2} + \frac{2m_{GH}\xi_2^2 L_{HI}}{\varepsilon^2},$$

$$K = 2\left(\frac{K_{rA}}{\varepsilon^2} + \frac{K_{rB}(a-1)^2}{\varepsilon^2} + \frac{K_{rC}(c-a-1)^2}{\varepsilon^2} + \frac{K_{rD}(c-1)^2}{\varepsilon^2} + \frac{K_{rE}(b-a)^2}{\varepsilon^2} + \frac{K_{rF}b^2}{\varepsilon^2} + \frac{K_{rG}\xi_1^2}{\varepsilon^2} + \frac{K_{rH}\xi_2^2}{\varepsilon^2} + \frac{K_{rI}\xi_3^2}{\varepsilon^2}\right) + k_{SPCA}$$

and $F = 2F_{in} - R_{amp}F_{out}$.

The working mode frequency can be obtained by

$$f = \frac{1}{2\pi}\sqrt{\frac{K}{M}} \quad (56)$$

D. Optimization design

High bandwidth (natural frequency) is important for the microgripper to perform high speed operations, and the initial dynamic analysis using ANSYS software is conducted first to investigate the vibration modes of the proposed microgripper. An initial microgripper are designed and the dimensions of the microgripper model are shown in Table I, where t=r_1=r_2=0.5mm. The dynamic analysis result shows that the first vibration mode is one of the local vibration caused by the linkages IJ and I'J', and the second vibration mode is the working mode, so the working mode frequency f is selected as the objective function for the optimization. Based on the static and dynamic models, the key parameters t, r_1 and r_2, are chosen as the design variables and defined within certain scope considering the actual applications and manufacturing conditions. The input stiffness k_{in} is a key factor that affects the characteristics of the microgripper. If k_{in} is large enough, good dynamic characteristics can be achieved. On the other hand, it can reduce the output displacement of the SPCA, so we define $k_{in} \le 20\%k_{SPCA}$. In addition, the maximum stress during working process should be less than the yield strength of the material.

TABLE I
THE INITIAL MODEL OF THE MICROGRIPPER

Parameters	L_1	L_2	L_3	L_4	L_5	L_6	L_7	L_8	L_9	L
Value (mm)	1	6	3	3.8	9.5	11.5	3.8	2	5	20

Optimization design has been carried out to improve the performance of the microgripper, and the optimization work can be concluded as follows:

1) Objective: Maximize the working mode frequency (f).
2) Related parameters: t, r_1 and r_2.
3) Subject to:
   a) input stiffness value: $k_{in} \le 20\%k_{SPCA}$ (k_{SPCA}=60 N/um);
   b) constraint equations: Eq. (51), and here n_a=2;
   c) parameter ranges: 0.2mm≤t≤0.5mm, 0.3mm≤r_1≤1mm, and 0.5mm≤r_2≤1mm.

Through optimization using MATLAB Optimization toolbox with the initial values x= [t, r_1, r_2]=[0.5,0.5,0.5], the optimization result is obtained as follows: t=0.2 mm, r_1=0.4 mm, r_2=0.9 mm, R_{amp}=14.2, k_{in}=3.32 N/μm and the working mode frequency f=970 Hz.

IV. CHARACTERISTIC ANALYSIS

The characteristics of the optimized microgripper are investigated using ANSYS software based on finite element analysis (FEA).

The deformation behavior of the jaws as well as flexure hinges and moving linkages under the input displacement of 10μm applied by the SPCA is calculated. The result shows that the maximum displacement of a jaw can reach 126 μm which can enable grasping operations with a large range of micro objects. The displacement amplification ratio of one gripping jaw is 12.6. The displacement amplification ratio by FEA is smaller than the mathematical amplification ratio of 14.2 because that the displacement loss effect arising from the combination of lever arm bending and connection flexure stretching will cause the actual lever amplification ratio to be smaller than the ideal value. The maximum stress generated at the flexure hinge D is 182MPa and it is less than the yield strength (503MPa) of the material. Figure 5 depicts the range of grasping clearances for the gripper jaws by FEA.

The grasping force is estimated by FEA, and the results are shown in Fig.6, where D is the initial distance between the jaws, d is the micro object diameter and δ is the distance between the jaw and micro objects. Before the jaws contact with the micro objects, the grasping force is zero, and the grasping force

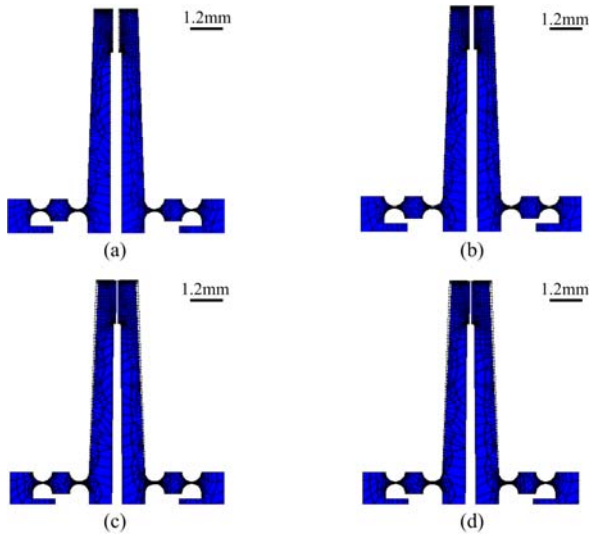

Fig. 5. Deformation behavior of the piezoelectric actuated microgripper with different grasping clearences for the gripper jaws by FEA. (a) 400μm, (b) 300μm, (c) 200μm and (d) 150μm.

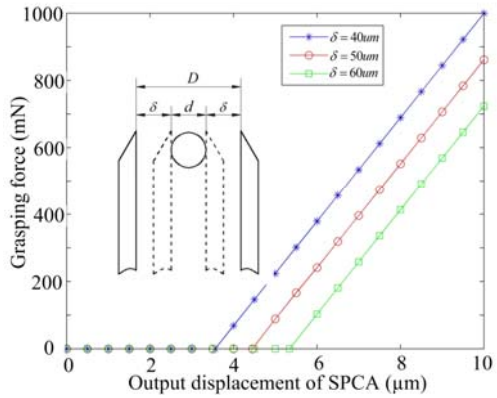

Fig. 6. The grasping force estimated by FEA.

increases linearly with the increase of the SPCA output displacement after contact. The grasping force can reach up to 1000 mN when the SPCA output displacement S_S is 10 μm and $\delta = 40\mu m$.

Through-modal analysis, the first two natural frequencies and corresponding mode shapes of the microgripper are obtained. The first mode shape of the microgripper is a kind of local vibration mode where the jaws vibrate in the same direction and the corresponding frequency is 842 Hz. The second mode shape shows the jaws vibrate in the opposite directions and the corresponding frequency is 986 Hz.

V. Experiments

Figure 7 shows the prototype of the microgripper driven by a SPCA (type: XP 5×5/18, output displacement: 0–18μm, applied voltage: 0–150V). The microgripper was fabricated through wire EDM to guarantee the geometrical accuracy of the crucial section of the gripper, and it was made from AL7075-T651with a high elasticity, yield strength, and light mass.

The experimental setup is displayed in Fig. 8, and it was mainly composed of the developed microgripper, laser displacement sensors (LK-H050 from Keyence, Inc) with an accuracy of 0.025μm and the voltage control unit including the PI voltage amplifier, dSPACE DS1103 controller, universal interface and the computer. The basic operation of the system was realized by applying the desired voltage from the voltage control unit to the SPCA to activate the output motion at the microgripper tip. By changing the driving voltage, stable operations were offered to implement continuous expansion and retraction motions.

Experiments were carried out to evaluate the grasping capacity of the microgripper through grasping gold wires. The grasping process was captured by a super depth 3D analysis system (VHX-1000 from Keyence, Inc) with a high pixel resolution. Figure 9 provides the grasping process of a gold wire with a diameter of 25.4 μm.

Figure 10 summarizes the tip displacements of one grasping microgripper jaw vary with the input displacement obtained by different approaches. The experimental measured displacement amplification ratio is 11.4 for one gripping jaw, which is in good agreement with the results by mathematical calculation and FEA, so the total displacement amplification ratio of the microgripper is 22.8.

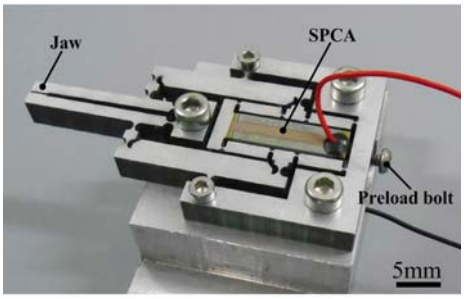

Fig. 7. The microgripper.

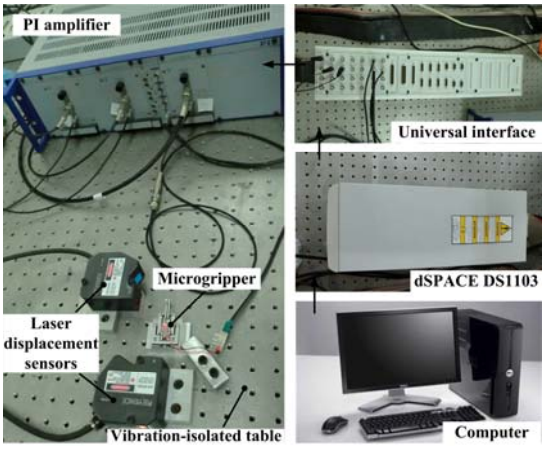

Fig. 8. Experimental setup of the microgripper.

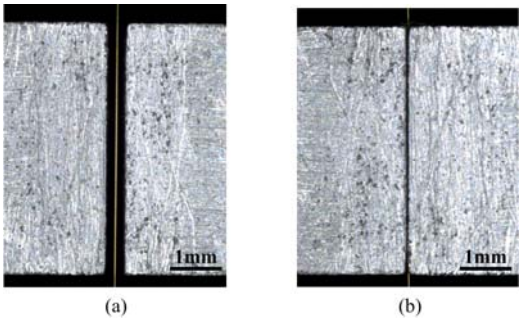

Fig. 9. Gasping the gold wire. (a) before grasping, and (b) after grasping.

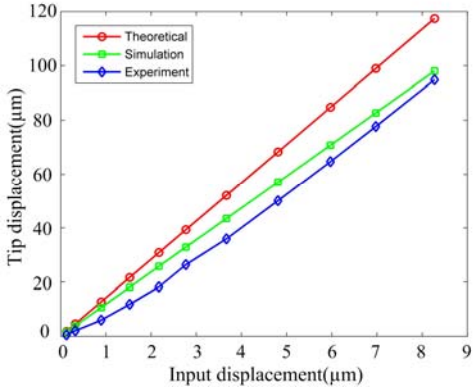

Fig. 10. Relationships between the tip displacement of one microgripper jaw and the input displacement obtained by different approaches.

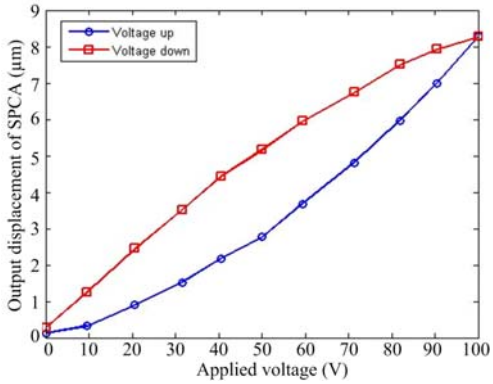

Fig. 11. SPCA Output displacement versus the applied voltage.

Figure 11 shows the SPCA output displacement versus the applied voltage, which exhibits the hysteresis behavior caused by the crystalline polarization effect and SPCA molecular friction. The maximum SPCA output displacement is 8.38μm under a 100V voltage signal provided.

Figure 12 shows a single jaw tip displacement versus the applied voltage. The maximum tip displacement of a single jaw is 95 μm corresponding to the 100 V applied voltage, and the motion stroke of microgripper can reach up to 190 μm.

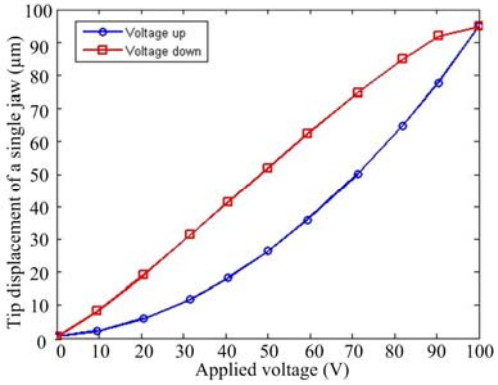

Fig. 12. Tip displacement of a single jaw versus the applied voltage.

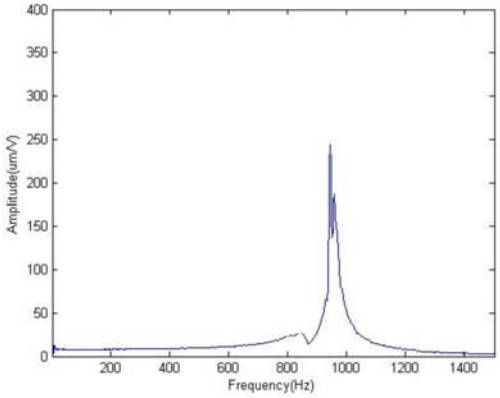

Fig. 13. The transfer function of dynamic measurements.

TABLE II
COMPARASION WITH OTHER MICROGRIPPERS

Actuation	Motion stroke (μm)	Amplification ratio	Force (mN)	Reference
PZT	134	15.5	-	[24]
PZT	100	3.68	950	[25]
PZT	-	16	110	[26]
Electrostatic	130	-	0.38	[11]
Electrothermal	13	-	-	[14]
PZT	190	22.8	1000 (S_S=10; $\delta = 40\mu m$)	This work

The resonance frequency of the microgripper was tested by applying a swept sine signal to the SPCA. In the experiment, the microgripper was driven by a voltage with amplitude of 20V and a frequency from 0.01 to 1500 Hz. The transfer function is shown in Fig.13. The vibration modes of the microgripper were observed using the super depth 3D analysis system (VHX-1000 from Keyence, Inc). The result shows that the working vibration mode is excited and the corresponding frequency is 953 Hz, which is consistent with the results by the mathematical calculation of 970 Hz and FEA of 986 Hz.

Table II summarizes the comparasion with other related

microgrippers, and the results show that the microgripper has a larger motion stroke, amplification ratio and force compared with others.

VI. Conclusion

Design, modeling, fabrication and experimental test of a novel piezoelectric actuated microgripper have been reported in this paper. A large displacement amplification ratio has been achieved through a three-stage flexure-based amplification. By use of the PRBM and Lagrange approaches, the kinematic, static, and dynamic models have been established first, and then the dimensions of the microgripper has been determined through optimization design with considerations of the crucial parameters that determine the characteristics of the microgripper including the working mode frequency, the input stiffness and the maximum stress. The static and dynamic characteristics of the microgripper have been analyzed using FEA and the prototype of the microgripper has been manufactured through wire EDM. Experimental tests have been implemented to examine the performance of the microgripper, and the results show that the total amplification ratio of the microgripper is 22.8, and the motion stroke of microgripper can reach up to 190 μm corresponding to the 100 V applied voltage. The working mode frequency of the microgripper is 953 Hz. The microgripper has successfully grasped gold wires. Future work will focus on the modeling and compensation of the hysteresis behavior of the microgripper, and output force measurement, calibration and control.

References

[1] Y.M. Li, and Q. S. Xu, "Design and robust repetitive control of a new parallel-kinematic XY piezostage for micro/nanomanipulation," *IEEE/ASME Trans. Mechatronics*, vol. 17, no. 6, pp. 1120–1132, Dec. 2012.

[2] G.Y. Gu, L.M. Zhu, C.Y. Su, and H. Ding, "Motion control of piezoelectric positioning stages: modeling, controller design and experimental evaluation," *IEEE/ASME Trans. Mechatronics*, vol. 18, no. 5, pp. 1459–1471, Oct. 2013.

[3] H. Zhang, F. Wang, Y. Tian, X. Zhao, and D. Zhang, "Electrical matching of low power piezoelectric ultrasonic transducers for microelectronic bonding," *Sens. Actuators A-Phys.*, vol. A199, no. 1, pp. 241-249, Sep 2013

[4] F. Wang, X. Zhao, D Zhang, Z Ma, and X. Jing, "Robust and precision control for a directly-driven XY table," *Proc. Inst. Mech. Eng. Part C J. Mech. Eng. Sci.*, vol, 225, pp. 1107-1120, May 2011.

[5] Y. Qin, B. Shirinzadeh, Y. Tian, and D. Zhang, "Design and computational optimization of a decoupled 2-DOF monolithic mechanism," *IEEE/ASME Trans. Mechatronics*, vol. 19, no. 3, pp. 872–881, June 2014.

[6] F. Wang, Z. Ma, W. Gao, X. Zhao, Y. Tian, D. Zhang, and C. Liang, "Dynamic modeling and control of a novel XY positioning stage for semiconductor packaging," *Transactions of the Institute of Measurement and Control*, [Online]. Available: http://tim.sagepub.com/content/early, DOI: 10.1177/0142331214541598.

[7] F. Wang, J. Li, S. Liu, X. Zhao, D. Zhang, and Y Tian, "An improved adaptive genetic algorithm for image segmentation and vision alignment used in microelectronic bonding," *IEEE/ASME Trans. Mechatronics*, vol. 19, no. 3, pp. 916-923, June 2014.

[8] A. Nkoonbin, and M. Hassani Niaki, "Deriving and analyzing the effective parameters in microgrippers performance," *Sharif University of Technology Scientia Iranica Transaction B: Mechanical Engineering*, vol. 19, no. 6, pp. 1554-1563, Dec. 2012.

[9] M.N.M. Zubir, B. Shirinzadeh and Y.L. Tian, "Development of a novel flexure-based microgripper for high precision micro-object manipulation," *Sens. Actuators A, Phys.*, vol. 150, no. 2, pp. 257-266, Mar. 2009.

[10] M.N.M. Zubir, B. Shirinzadeh and Y.L. Tian, "A new design of piezoelectric driven compliant-based microgripper for micromanipulation," *Mechanism and Machine Theory*, vol. 44, pp. 2248-2264, Dec. 2009.

[11] F. Beyeler, A. Neild, S. Oberti, D. J. Bell, Y. Sun, J. Dual, and B.J. Nelson, "Monolithically fabricated microgripper with integrated force sensor for manipulating microobjects and biological cells aligned in an ultrasonic field," *Journal of Microelectromechanical System*, vol. 16, no. 1, pp. 7-15, Feb. 2007.

[12] T. Chen, L. Chen, L. Sun, and X. Li, "Design and fabrication of a four-arm-structure MEMS gripper," *IEEE/ASME Trans. Electronics*, vol. 56, no. 4, pp. 996-1003, Apr. 2009.

[13] K. Kim, X. Liu, Y. Zhang, and Y. Sun, "Nanonewton force-controlled manipulation of biological cells using a monolithic MEMS microgripper with two-axis force feedback," *Journal of Micromechanics and Microengineering*, vol. 18, no. 5, pp. 1–8, 2008.

[14] N. Chronis, and L.P. Lee, "Electrothermally activated SU-8 microgripper *for single cell manipulation in solution*," *Journal of Microelectromechanical Systems*, vol. 14, no. 4, pp. 857–862, Aug. 2005.

[15] M. Kohl, E. Just, W. Pfleging, and S. Miyazaki, "SMA microgripper with integrated antagonism," *Sens. Actuators A-Phys.*, vol. A83, no. 1-3, pp. 208-213, May 2000.

[16] I. Roch, P. Bidaud, D. Collad, and L. Buchaillot, "Fabrication and characterization of an SU-8 gripper actuated by a shape memory alloy thin film," *J. Micromech. Microeng.*, vol. 13, pp. 330-336, 2003.

[17] S.K. Nah, and Z.W. Zhong, "A microgripper using piezoelectric actuation for micro-object manipulation," *Sens. Actuators A-Phys.*, vol. A133, no. 1, pp. 218-224, Jan. 2007.

[18] M. Grossard, C. Rotinat-Libersa, N. Chaillet, and M. Boukallel, "Mechanical and control-oriented design of a monolithic piezoelectric microgripper using a new topological optimization method," *IEEE/ASME Trans. Mechatronics*, vol. 14, no. 1, pp. 32-45, Feb. 2009.

[19] Y. Haddab, N. Chaillet, and A. Bourjault, "A microgripper using smart piezoelectric actuators," in *Proc. 2000 IEEE/RSJ International Conference on Intelligent Robots and Systems*, Oct. 2000, pp. 659-664.

[20] G. Gu, L. Zhu, and C. Su, "Integral resonant damping for high-bandwidth control of piezoceramic stack actuators with asymmetric hysteresis nonlinearity," *Mechatronics*, vol.24, no.4, pp. 367-375, June 2014.

[21] G. Gu, L. Zhu, and C. Su, "Modeling and compensation of asymmetric hysteresis nonlinearity for piezoceramic actuators with a modified Prandtl-Ishlinskii model," *IEEE Transactions on Industrial Electronic*s, vol.61, no.3, pp. 1583-1595, March 2014

[22] G. Gu, M. Yang, and L. Zhu, "Real-time inverse hysteresis compensation of piezoelectric actuators with a modified Prandtl-Ishlinskii model," *Review of Scientific Instruments*, vol.83, no.6, pp. 065106, June 2012.

[23] Y.C. Tsai, S.H. Lei, and H. Sudin, "Design and analysis of planar compliant microgripper based on kinematic approach", *J. Micromech. Microeng.*, vol, 15, no.1, pp. 143-156, 2005.

[24] X. Sun, W. Chen, Y. Tian, S. Fatikow, R. Zhou, J. Zhang, and M. Mikczinski, "A novel flexure-based microgripper with double amplification mechanisms for micro/nano manipulation," *Rev Sci Instrum.*, vol. 84, no. 8, pp. 085002, 2013.

[25] M.N.M. Zubir, B. Shirinzadeh and Y.L. Tian, "Development of a novel flexure-based microgripper for high precision micro-object manipulation," *Rev Sci Instrum.*, vol. 80, no. 6, pp. 065106, 2009.

[26] D.H. Wang, Q. Yang, and H.M. Dong, "A monolithic compliant piezoelectric-driven microgripper: design, modeling, and testing," *IEEE/ASME Trans. Mechatronics*, vol. 18, no. 1, pp. 138-147, Feb. 2013.

[27] D. Handley, T. Lu, Y. Yong, and W. Zhang, "A simple and efficient dynamic modeling method for compliant micropositioning mechanisms using flexure hinges, in *Proc. SPIE International Symposium on Microelectronics, MEMS, and Nanotechnology*, Dec 2003, pp. 67-76.

Fujun Wang received the B.Eng. degree in mechanical manufacturing and automation from Hebei University of Technology, Tianjin, China, in 2005, and the M.Sc. and Ph.D. degrees in mechanical manufacturing and automation from Tianjin University, Tianjin, China, in 2007 and 2010, respectively.

He became an assistant professor in the School of Mechanical Engineering, Tianjin University in 2010. Now he is also a research scholar in the Center for Nanoscale Chemical-Electrical-Mechanical Manufacturing Systems, Department of Mechanical Science and Engineering, University of Illinois at Urbana-Champaign, Urbana, USA. His current research interests include micro/nano manipulation and positioning techniques, micro/nano manufacturing, dynamics and control, flexure actuator and robots.

Cunman Liang received the B.Eng. degree in mechanical manufacturing and automation in the School of Mechanical Engineering, Tianjin University, Tianjin, China, in 2010, where he is currently working towards the M.Sc. degree.

His current research interests include high speed and high precision manipulation, flexure mechanisms, dynamic and control.

Yanling Tian received the B.Eng. degree in mechanical engineering from Northwest Institute of Light Industry, Xianyang, China, in 1997, and the M.Sc. and Ph.D. degrees in mechanical engineering from Tianjin University, Tianjin, China, in 2002 and 2005, respectively.

From 2005 to 2006, he was a Postdoctoral Research Fellow at Tianjin University, where he has been appointed as a professor now. From 2007 to 2009, he was a Research Fellow in the Robotics and Mechatronics Research Laboratory, Department of Mechanical and Aerospace Engineering, Monash University, Australia. He was a Visiting Scholar at Hongkong University of Science and Technology, China, and the University of Warwick, U.K., in 2001 and 2006, respectively. He was also a Visiting Professor at Tohoku University, Japan, in 2010. He has accomplished a couple of government and industry-based projects, and published more than 50 peer-reviewed papers. He obtained the prestigious Alexander von Humboldt Fellowship for experienced researchers in 2010. His research interests include micro/nanomanipulation, mechanical dynamics, finite element method, surface metrology and characterization.

Xingyu Zhao received the B.Eng. and M.E. degrees from Hebei University of Technology in 1995 and 1998, respectively, and Ph.D. degree in mechanical manufacturing and automation from Tianjin University, Tianjin, China, in 2001.

Now she is an Associate Professor in the School of Mechanical Engineering, Tianjin University. Her current research interests are the kinematics and dynamics of parallel manipulators, finite element analysis, and micro/nanopositioning technique.

Dawei Zhang received the B.Eng. degree in mechanical engineering from Shenyang University of Technology, Shenyang, China, in 1984, and the M.Sc. and Ph.D. degrees in mechanical engineering from Tianjin University, Tianjin, China, in 1990 and 1995, respectively.

From 1984 to 1987, he was an Associate Engineer with the Tianjin Institute of Power Source, China. He is currently a Professor in the School of Mechanical Engineering, Tianjin University. His current research interests include micro/nanopositioning technique, structural dynamics, signal processing, high-speed machining methodologies, and dynamic design of machine tools.